Controlling the magnetoelectric coupling in Ni/BiFe0.95Mn0.05O3 with a dielectric spacer

Béatrice Negulescu, Jérôme Wolfman, Antoine Ruyter, Cécile Autret-Lambert, Salia Cherifi-Hertel

Controlling the magnetoelectric coupling in Ni/BiFe0.95Mn0.05O3 with a dielectric spacer

Béatrice Negulescu, Jérôme Wolfman, Antoine Ruyter, Cécile Autret-Lambert, Salia Cherifi-Hertel

Controlling the magnetoelectric coupling in Ni/$BiFe_{0.95}Mn_{0.05}O_3$ with a dielectric spacer

Beatrice Negulescu[1], Jérôme Wolfman[1], Antoine Ruyter[1], Cécile Autret-Lambert[1], Salia Cherifi-Hertel[2]

[1]Université de Tours, CNRS, GREMAN, UMR 7347, 37200 Tours, France

[2] Université de Strasbourg, CNRS, IPCMS, UMR 7504, 67000 Strasbourg, France

Highlights :

- Reversible and non-volatile magnetoelectric effect in bismuth ferrite based heterostructure.
- Large modulation of the magnetic coercive field by electric field.
- Strain-mediated magnetoelectric coupling mechanism.
- Control of the depolarizing field by an interleaved dielectric spacer.
- Volatile to non-volatile tuning of the magnetoelectric response through the depolarizing field.

Controlling the magnetoelectric coupling in Ni/$BiFe_{0.95}Mn_{0.05}O_3$ with a dielectric spacer

Beatrice Negulescu[1], Jérôme Wolfman[1], Antoine Ruyter[1], Cécile Autret-Lambert[1], Salia Cherifi-Hertel[2]

[1]Université de Tours, CNRS, GREMAN, UMR 7347, 37200 Tours, France

[2] Université de Strasbourg, CNRS, IPCMS, UMR 7504, 67000 Strasbourg, France

Abstract

In artificial multiferroic heterostructures combining ferromagnetic transition metal films and bismuth ferrite layers the electric field control of the magnetic state is generally achieved through interface exchange coupling. Here we report a reversible and non-volatile magnetoelectric (ME) effect in Ni/$BiFe_{0.95}Mn_{0.05}O_3$ bilayers originating primarily from a strain-transfer mechanism. The non-volatility of the ME effect is explained by an asymmetric piezoelectric strain response of the ferroelectric $BiFe_{0.95}Mn_{0.05}O_3$ film with respect to the applied electric field, yielding two different states at remanence. We further show that the piezoelectric properties and the ferroelectric domain structure of the $BiFe_{0.95}Mn_{0.05}O_3$ film can be controlled by tuning the screening of the polarization charge at the interface through an interleaved dielectric $SrTiO_3$ spacer. As the dielectric spacer thickness is decreased, the strain-mediated ME response evolves from the typical butterfly-like hysteresis loop towards a rectangular shape, thereby making such artificial multiferroics suitable for non-volatile memory applications.

Introduction

The electric field control of the magnetic state in multiferroic heterostructures, such as ferromagnetic (FM) / ferroelectric (FE) bilayers, occurs through strain-mediated mechanisms and interface-related effects [1-6]. The strain-mediated magnetoelectric (ME) coupling is due to the converse piezoelectric effect and magneto-elastic interactions and may result in a strong electric field control of the magnetic anisotropy [7-12]. The interface-related ME coupling mechanisms can typically be either exchange-related [13-16], triggered by the ionic mobility at the interface [17-18], or electronically-driven [19-22]. In spite of the efforts being made to achieve large ME coupling at interfaces [23-26], the overall coupling strength remains low. Alternatively, strain-mediated coupling involves a large volume fraction of the heterostructure, leading to a greater voltage-driven modulation of the magnetic state.

The strain-related mechanism typically induces a symmetric variation of the magnetization with respect to the applied electric field (i.e., a butterfly-like ME curve) that mimics the strain curve of the FE material [7], [10]. The FE polarization reversal results in the same strain-induced magnetic state at remanence for both the positive and negative voltage branches, which renders this effect unsuitable for non-volatile memory applications. Recent studies have shown that asymmetric polarization curves [27-28] and specific polarization reversal paths related to the FE domain structure [29-32] provide a possibility to break the symmetry of ME curves in strain coupled heterostructures.

Here we evidence a strain-mediated coupling in Ni/$BiFe_{0.95}Mn_{0.05}O_3$ (BFMO) bilayers by combining magneto-optic and piezoelectric measurements. Interleaving a thin dielectric $SrTiO_3$ (STO) film between Ni and BFMO shed light on the origin of the ME coupling in this system by disregarding direct interface effects. Furthermore, a controlled transition of the ME curve from a rectangular shape

hysteresis loop with two non-volatile remanent states to a conventional butterfly-like hysteresis loop is obtained by tuning the thickness of the dielectric spacer. Piezo-response force microscopy (PFM) reveals that the dielectric STO layer modifies the domain structure of the BFMO films. Recent studies have shown that the control of bound charge screening is capable of stabilizing exotic topological structures such as polar vortices [33], skyrmions [34] and bubble domains [35] in FE/ dielectric heterostructures. We consider that the control of the FE state through the depolarizing field can represent a new degree of freedom for tuning the ME coupling in ferromagnetic/ dielectric/ ferroelectric heterostructures.

Materials end methods

Pulsed laser deposition was used to grow $BiFe_{0.95}Mn_{0.05}O_3$ (60 nm)/ $La_{0.8}Sr_{0.2}MnO_3$ (25 nm) epitaxial stack on (110)-oriented $GdScO_3$ substrate. Mn doping of the $BiFeO_3$ structure was used in order to reduce the high leakage currents generally observed in the $BiFeO_3$ thin films [36-38]. The deposition conditions were 0.2 mbar oxygen pressure, 700 °C substrate temperature, and 1.72 $J{\cdot}cm^{-2}$ laser fluence. The films were cooled down at a rate of 3 °C/min in 500 mbar O_2 atmosphere after deposition. In one sample a STO wedge was deposited on top of the BFMO film, with thickness varying from 0 to 7 nm, to evaluate the interface contribution to the ME coupling. The STO deposition conditions were 0.03 mbar oxygen pressure, 700 °C substrate temperature and 1.72 $J{\cdot}cm^{-2}$ laser fluence. 30 nm-thick Ni films were subsequently grown by e-beam evaporation using standard lithography and lift-off process. The magnetic film was capped with 10 nm Au to prevent from oxidation. Two additional samples with 5 nm and 10 nm Ni thicknesses were prepared to study the Ni/BFMO interface contribution to the ME coupling process. The $La_{0.8}Sr_{0.2}MnO_3$ (LSMO) and BFMO films have a single crystalline structure while the Ni layers are polycrystalline. X-ray diffraction measurements and transmission electron microscopy images are provided as supplementary material (see supplementary figure S1). A detailed structural characterization of the heterostructure was presented elsewhere [39].

The magnetic properties were measured using magneto-optic Kerr effect (MOKE) in the longitudinal mode using a NanoMOKE system from Durham Magneto Optics. The Ni top electrodes used for the magnetic measurements have a circular geometry (20 µm diameter) while deported rectangular pads (50x50 μm^2) have been used for applying the electric voltage between the Ni film and the LSMO (bottom electrode) using a Keithley 2410 source/measure unit, as schematically represented in Figure 1a. The magnetic anisotropy was investigated after removing the DC bias (i.e., in the remanent FE state), by varying the azimuth angle of the sample with respect to the applied magnetic field. PFM with a commercial scanning probe microscope (Dimension 3100, Bruker) in contact mode was used to image the FE domain structure. The piezoelectric properties of the BFMO films were analyzed by double beam laser scanning vibrometry (LSV) using a MSA 500 laser Doppler vibrometer equipped with a VD-06 high precision velocity decoder from Polytech. The vibrometry method use an interferometric optical detection of the conversed piezoelectric effect generated by an AC voltage (0.5 V at 10 kHz for these measurements). The vertical displacement detected by the LSV is therefore proportional to the polarization. By means of a DC bias in parallel with the AC excitation signal, the FE polarization can be modulated. $d_{33}(V_{DC})$ loops obtained by LSV measurements were used to characterize the polarization reversal of the BFMO film, where the d_{33} piezoelectric tensor element values were calculated as the vertical displacement amplitude divided by the AC excitation amplitude. These loops are similar to the amplitude-voltage curves obtained by PFM measurements, with the main difference that PFM probes

the kinetics of nanoscale domain switching, while LSV describes the FE switching averaged over the entire electrode area.

Results and discussions

Figure 1b displays the magnetic hysteresis loops measured in the as deposited state and after poling the system at ±6 V (corresponding to an electric field of ±1000 kV/cm). The electric remanent states of the heterostructure are referred to as positively or negatively poled state, depending on the sign of the applied voltage. A small coercive field Hc = 20 Oe is observed in the as-grown virgin state. The coercivity drastically increases to 120 Oe upon positive poling (500 % variation) and it remains unchanged after the voltage is switched-off. The negative poling reduces the coercivity to about 40 Oe, which is higher than the initial value, but represents 200 % variation with respect to the positively poled state. Small variations of the saturation magnetization (Ms) upon poling are also observed (see MOKE signal intensity in Figure 1b). These results are characteristic of a strong ME coupling in Ni/BFMO bilayers, in agreement with our previously reported results [40]. The magnetic anisotropy variation with the electric field was investigated by measuring the in-plane angular dependence of the magnetization curves for different poling states. The polar plots of the coercive field and of the normalized remanent magnetization (Mr/Ms) derived from these measurements are presented in Figure 1c and d, respectively. Unpoled bilayers exhibit a small uniaxial anisotropy (see elongated lobes in Figure 1c,d) that is lost at positive poling and recovered at negative poling.

To understand the role of interface effects on the studied ME coupling, we interleaved a dielectric STO spacer with variable thicknesses between Ni and BFMO layers. The magnetic coercivity modulation between the positively and the negatively poled states, ΔHc, is used in Figure 2 to analyze the influence of the STO spacer thickness on the ME effect. For the thinner part of the spacer, a linear decrease of ΔHc is observed as the STO thickness increases up to a threshold value of about 4 nm. Above 4 nm STO, the coercivity difference between the two poled states vanishes. It is worth mentioning that the coercivity in the as deposited state is independent of the STO thickness and that positive poling results in an increased coercivity in the whole STO thickness range (results presented in supplementary Figure S2).

The ME coupling and its origin is further investigated in the following by comparing the effect of the voltage cycling on the magnetic properties (Hc and Ms) to the piezoelectric response of Ni/STO/BFMO heterostructures (Figure 3). We observe a gradual change of the ME curves shape from a rectangular hysteresis loop to a butterfly-like loop, depending on the thickness of the STO spacer (see Figure 3a,b). In the absence of the STO spacer, the ME curves show a pure rectangular hysteresis shape, with two distinct remanent Hc and Ms values. Typical butterfly-like curves are obtained when 5.5 nm thick STO is interleaved. In this case, equivalent remanent Hc and Ms values are found for positive and negative voltage branches. At an intermediate STO spacer thickness of 2 nm, the ME curves present mixed rectangular and butterfly shapes, with two different remanent magnetic states.

Close similarity is observed between the magnetic Hc(V) and Ms(V) curves and the piezoelectric d_{33}(V) response (presented in Figure 3c). The heterostructure without STO spacer is characterized by a sharp decrease of the piezoelectric response to zero in both positive and negative branches, associated to the FE polarization reversal. The bias voltage at which the BFMO polarization is reversed clearly corresponds to the transition between the high and low Hc (Ms) states presented in Figure 3a(b). However, some features of the d_{33}(V) curve are difficult to explain just considering a typical FE polarization reversal process, such as the large increase of the d_{33} value when the DC voltage is reduced

from +6 V (11 pm/V) to 0 V (25 pm/V). A large asymmetry can also be observed between the two branches of the d_{33}(V) curve, showing two different piezoelectric remanent states. In fact, two distinct contributions have to be considered in the piezoelectric response of a FE material. One is related to the intrinsic piezoelectric effect (i.e. due to the lattice deformation) and the second one, also known as extrinsic response, is induced by the domain wall (DW) motion [41]. The large asymmetry observed between the two branches of the d_{33}(V) curve indicates different strain states in the BFMO film that may result from dissimilar FE domain structures (i.e. difference between the DWs type and/or density). This asymmetry is likely at the origin of the rectangular shape ME response.

In the case of a 5.5 nm STO spacer, a conventional butterfly-like d_{33} loop shape is obtained, which is the typical strain response to electric field of a FE system. The butterfly-like shape of the ME response in the case of thick STO spacer (Figure 3a,b) reflects thus the d_{33} loop shape, as expected for a strain-mediated coupling mechanism [7], [10], [42], [43]. At intermediate STO thicknesses (e.g., 2 nm), the d_{33} loop deviates from the butterfly-like shape and shows a gradual FE switching as d_{33} goes to zero and recovers slowly with the applied bias. This gradual FE switching affects the corresponding Hc and Ms loops that show a mixed butterfly and rectangular hysteresis shape. In conclusion, our results show a clear correlation between the piezoelectric and the ME responses, indicating the presence of strain-mediated effect in the studied system.

Although the STO spacer revealed the effects of strain-mediated coupling, we need to consider the possibility of additional coupling mechanisms in the case of Ni/BFMO bilayers (i.e., without STO spacer). Besides, the STO thickness induced change of the ME curve shape from butterfly to rectangular could also suggest the coexistence of several coupling mechanisms [43]. Electronically driven charge effect can be discarded in the studied system, because the thickness of the Ni film (30 nm) is much larger than the Thomas-Fermi screening length (less than 1 nm). Previous reported X-ray photoemission spectroscopy and electron energy-loss spectroscopy analysis of the Ni/ BFMO interface did not reveal any electric field dependent redox effect in this system [39]. Therefore, ionic mobility under electric field can be excluded in the Ni/ BFMO bilayers. Furthermore, the investigation of the FM thickness influence on the ME coupling didn't show a monotonic variation of the ME properties as a function of the Ni thickness (see Supplementary Figure S3), as expected in interface-mediated coupling mechanisms such as exchange coupling [44]. We should mention here that exchange bias is not expected in the Ni/BFMO system as the Ni film is not deposited under magnetic field. Exchange coupling should therefore manifest through an increase of the Hc values, as observed in several other BFO based systems [15-16]. The magnetic coercivity modulation between the positively and the negatively poled states is not sensitive to the thickness of the Ni film, which does not sustain an exchange coupling origin of the studied ME effect. Moreover, in view of the rather thick Ni film used in this study, we consider that exchange coupling effect can be ignored in Ni (30 nm)/ BFMO bilayers. In summary, interface-related ME coupling mechanisms can be ruled out, which leaves strain transfer as the predominant ME coupling mechanism in the studied system.

The ME effect in strain-coupled structures generally modifies the magnetic anisotropy [8-12]. In the Ni/BFMO bilayers the ME coupling results in a huge variation of Hc. The coercive field is not a direct measurement of the magnetic anisotropy but characterizes the reversed magnetic domain nucleation process, as well as the motion of the magnetic DWs during the magnetization reversal. The strong variation of Hc with the applied voltage observed in the Ni/BFMO bilayers may thus result from a modification of the magnetic DWs pinning sites. This effect can be induced by local strains developed

in the BFMO film after the FE switching. Three polarization switching paths have been reported in rhombohedral perovskite materials such as BFMO, namely 71°, 109°, and 180°. Only the 109° switching events create in plane distortions along the [110] and the [-110], which could locally modify the strain in the Ni film [29-30], [32].

Let us now discuss the possible microscopic origin of the transition from rectangular shape to butterfly-like shape of the piezoelectric loops with the thickness of the dielectric spacer. The dielectric STO spacer may strongly affect both the FE domain configuration and the polarization switching process, as already reported in $PbTiO_3$/ STO [45-46], $Pb(Zr_{0.2}Ti_{0.8})O_3$/ STO [47], and $BiFeO_3$/ $LaBiFeO_3$ [48] heterostructures. PFM was used to investigate the FE domain structure of the BFMO films with and without STO capping. Bare BFMO films do not show any contrast in the vertical PFM images, indicating a single polarization orientation respectively to the out of plane direction. During the PFM measurements the reversal of the BFMO polarization was achieved by applying a positive voltage on the tip (see supplementary Figure S4), which means that the polarization of the as deposited film is oriented towards the LSMO electrode. A multi-domain structure with up and down polarization is observed in STO capped BFMO films (see Figure 4). The transformation of the FE domain structure is controlled by the STO layer through the surface charge screening of the polarization (i.e., via the control of the depolarizing field). Different polarization reversal routes and piezoelectric characteristics are therefore expected, depending on the STO spacer thickness.

In order to understand how the FE domain configuration influences the shape of the ME loops, we should first note that the Ni film is unstrained in the as deposited state, independently of the BFMO domain structure (see figure S3 for the Hc variation with the STO thickness). The unstrained Ni film is characterized by a low Hc value of about 20 Oe. Without STO spacer, this initial state corresponds to a polarization orientation towards the LSMO bottom electrode. In positive bias the polarization reversal is associated with a certain amount of 109° switching events that generate local strained regions in the Ni film. Consequently, the magnetic coercive field increases to about 120 Oe (see figure 3a). The polarization reversal in negative bias brings the FE domain structure close to the initial one, thus reducing the strain state in the BFMO and Ni films. As a result, Hc decreases to 40 Oe. This behavior suppose that the initial FE domain structure is energetically favorable so that it is recovered after a switching cycle. Asymmetric FE states between the positive and the negative poling have been already reported for BFO thin films [49, 50] and were associated to the existence of interfacial defects acting as pinning centers for the as deposited FE domains.

With a STO top layer, the polarization of the as-grown FE film is oriented both upward and downward. This FE domain structure corresponds to a low strain state for Ni in the as-deposited Ni/STO/BFMO trilayer. When a positive voltage is applied, only the FE regions oriented toward the LSMO electrode are reversed. Consequently, the amount of 109° switching events is smaller than in the case of the structure without STO spacer and a reduced strain is transferred to the Ni film. As a result of this FE switching process Hc increases to about 70 Oe for the structure with 5.5nm thick STO spacer, value that is lower than the one observed in the Ni/BFMO bilayers (see figure 3a). When the positive bias is decreased to zero, the initial FE multi-domain structure is gradually recovered thus the strain and, correspondingly, the Hc value are reduced. The reversal of the polarization toward the LSMO electrode in negative bias now switches the FE domains that were initially oriented upward. In consequence, the strain increases in the Ni film inducing an increased value of Hc. In this FE switching process, similar strain states are expected in positive and negative bias, thus inducing symmetric ME curves.

Let us now discuss the effect of the electric field on the magnetic anisotropy. The as deposited Ni film shows a small uniaxial anisotropy with the magnetic easy axis oriented along the [100] direction (see Figure 1c,d). In positive bias, the FE polarization reversal generates local in plane distortions along the [110] and the [-110] directions. Transferred to the adjacent Ni film, this strain should locally induce the magnetic easy axis reorientation. The lateral dimension of this strained regions correspond to that of the FE domains, which is on the order of 100 nm (see supplementary figure S4). In comparison, the MOKE is sensitive to a large area of the Ni film (laser spot focused at 5 µm). The magnetic response is therefore averaged over a large number of unstrained and locally strained regions, with different easy axis directions. This could explain the isotropic-like Mr/Ms and Hc polar plots observed in the positive poled state.

Conclusions

In summary, a non-volatile strain-mediated ME coupling was demonstrated in Ni/ BFMO bilayers. Interface-mediated coupling can be ruled out in this system and the non-volatility of the ME effect is correlated to bistable remanent strain state in BFMO. Interleaving a dielectric STO spacer between Ni and BFMO modifies the ferroelectric properties through the depolarizing field modulation. This directly impacts the piezoelectric curves and the related ME response. The thickness of the STO spacer controls the polarization charges screening and therefore tunes both the piezoelectric and the ME curves from the usual butterfly-like response to a rectangular shape loop with two non-volatile memory states. This result proves that the control of the ferroelectric properties through the depolarizing field is a promising route to fine-tune ME memory states in artificial multiferroics.

Acknowledgments

This work was funded by Région Centre in the frame of the project Comhet.

Supplementary material

See supplementary material for further detailed structural and magnetoelectric characterization of the studied system.

Data statement

The data used in this article are available from the corresponding author upon reasonable request.

References

[1] C. Song, B. Cui, F. Li, X. Zhou, F. Pan, Prog. Mater. Sci. 87, 33–82, (2017).

[2] J-M. Hu, L.-Q. Chen, C-W. Nan, Adv. Mater. 28, 15–39, (2016).

[3] F. Matsukura, Y.Tokura, H. Ohno, Nat. Nanotech. 10, 209-220, (2015).

[4] V. Garcia, M. Bibes, A. Barthélémy, C. R. Physique 16, 168–181, (2015).

[5] M. Liu, N.X. Sun, Phil. Trans. R. Soc. A 372, 20120439, (2014).

[6] C. A. F. Vaz, J. Phys.: Condens. Matter 24, 333201, (2012).

[7] C. Thiele, K. Dörr, O. Bilani, J. Rödel, L. Schultz, Phys. Rev. B 75, 054408, (2007).

[8] M. Weiler, A. Brandlmaier, S. Geprägs, M. Althammer, M. Opel, C. Bihler, H. Huebl, M. S. Brandt, R. Gross, S. T. B. Goennenwein, New J. Phys. 11, 013021, (2009).

[9] T. Wu, A. Bur, K. Wong, J. L. Hockel, C.-J. Hsu, H. K. D. Kim, K. L. Wang, G. P. Carman, J. Appl. Phys. 109, 07D732, (2011).

[10] J. Wang, J. Ma, Z. Li, Y. Shen, Y. Lin, C. W. Nan, J. Appl. Phys. 110, 043919, (2011).

[11] J. Cui, J. L. Hockel, P. K. Nordeen, D. M. Pisani, C.-Y. Liang, G. P. Carman, C. S. Lynch, Appl. Phys. Lett. 103, 232905, (2013).

[12] Z. Wang, Y. Wang, W. Ge, J. Li, D. Viehland, Appl. Phys. Lett. 103, 132909, (2013).

[13] P. Borisov, A. Hochstrat, X. Chen, W. Kleemann, C. Binek, Phys. Rev. Lett. 94, 117203, (2005).

[14] V. Laukhin, V. Skumryev, X. Marti, D. Hrabovsky, F. Sánchez, M.V. Garcia-Cuenca, C. Ferrater, M. Varela, U. Lüders, J.F. Bobo, J. Fontcuberta, Phys. Rev. Lett. 97, 227201, (2006).

[15] H. Béa, M. Bibes, S. Cherifi, F. Nolting, B. Warot-Fonrose, S. Fusil, G. Herranz, C. Deranlot, E. Jacquet, K. Bouzehouane, A. Barthélémy, Appl. Phys. Lett. 89, 242114, (2006).

[16] Y-H. Chu, L. W. Martin, M. B. Holcomb, M. Gajek, S-J. Han, Q. He, N. Balke, C-H. Yang, D. Lee, W. Hu, Q. Zhan, P-L. Yang, A. Fraile-Rodríguez, A. Scholl, S. X. Wang, R. Ramesh, Nat. Mat. 7, 478–482, (2008).

[17] C. Bi, Y. Liu, T. Newhouse-Illige, M. Xu, M. Rosales, J. W. Freeland, O. Mryasov, S. Zhang, S. G. E. Velthuis, W. G. Wang, Phys. Rev. Lett. 113, 267202, (2014).

[18] U. Bauer, L. Yao, A. Jun Tan, P. Agrawal, S. Emori, H. L. Tuller, S. van Dijken, G. S. D. Beach, Nat. Mat. 14, 174–181, (2015).

[19] C.-G. Duan, S. S. Jaswal, E. Y. Tsymbal, Phys. Rev. Lett. 97, 047201, (2006).

[20] J. M. Rondinelli, M. Stengel, N. A. Spaldin, Nat. Nanotech. 3, 46–50, (2008).

[21] C.-G. Duan, J. P. Velev, R. F. Sabirianov, Z. Zhu, J. Chu, S. S. Jaswal, E. Y. Tsymbal, Phys. Rev. Lett. 101, 137201, (2008).

[22] M. K. Niranjan, J. P. Velev, C.-G. Duan, S. S. Jaswal, E. Y. Tsymbal, Phys. Rev. B 78, 104405, (2008).

[23] J. D. Burton, E. Y. Tsymbal, Phys. Rev. B 80, 174406, (2009).

[24] G.Radaelli, D. Petti, E. Plekhanov, I. Fina, P. Torelli, B. R. Salles, M. Cantoni, C. Rinaldi, D. Gutiérrez, G. Panaccione, M. Varela, S. Picozzi, J. Fontcuberta, R. Bertacco, Nat. Commun. 5, 3404, (2014).

[25] I. R. Reddy, P. M. Oppeneer, K. Tarafder, Phys. Rev. B 98, 140401, (2018).

[26] R. Arras, S. Cherifi-Hertel, ACS Appl. Mater. Interfaces 11, 34399-34407, (2019).

[27] E. Menéndez, V. Sireus, A. Quintana, I. Fina, B. Casals, R. Cichelero, M. Kataja, M. Stengel, G. Herranz, G. Catalán, M. Dolors Baró, S. Suriñach, J. Sort, Phys. Rev. Applied 12, 014041, (2019).

[28] M. Foerster, I. Fina, S. Finizio, B. Casals, A. Mandziak, F. Fauth, L Aballe, J. Phys.: Cond. Matter 31, 084003, (2019).

[29] S. Zhang, Y. G. Zhao, P. S. Li, J. J. Yang, S. Rizwan, J. X. Zhang, J. Seidel, T. L. Qu, Y. J. Yang, Z. L. Luo, Q. He, T. Zou, Q. P. Chen, J.W. Wang, L. F. Yang, Y. Sun, Y. Z. Wu, X. Xiao, X. F. Jin, J. Huang, C. Gao, X. F. Han, R. Ramesh, Phys. Rev. Lett. 108, 137203, (2012).

[30] L. Yang, Y. Zhao, S. Zhang, P. Li, Y. Gao, Y. Yang, H. Huang, P. Miao Y. Liu, A. Chen, C. W. Nan, C. Gao, Sci. Rep. 4, 4591, (2014).

[31] Y. Liu, Y. Zhao, P. Li, S. Zhang, D. Li, H. Wu, A. Chen, Y. Xu, X. F. Han, S. Li, D. Lin, H. Luo, ACS Appl. Mater. Interfaces 8, 3784−3791, (2016).

[32] S. Zhang, Q. Chen, Y. Liu, A. Chen, L. Yang, P. Li, Z. S. Ming, Y. Yu, W. Sun, X. Zhang, Y. Zhao, Y. Sun, Y. Zhao, ACS Appl Mater Interfaces. 9, 20637-20647, (2017).

[33] A.Yadav, C. Nelson, S. Hsu, Z. Hong, J. D. Clarkson, C. M. Schlepütz, A. R. Damodaran, P. Shafer, E. Arenholz, L. R. Dedon, D. Chen, A. Vishwanath, A. M. Minor, L. Q. Chen, J. F. Scott, L. W. Martin, R. Ramesh, Nature 530, 198–201 (2016).

[34] S. Das, Y. L. Tang, Z. Hong, M. A. P. Gonçalves, M. R. McCarter, C. Klewe, K. X. Nguyen, F. Gómez-Ortiz, P. Shafer, E. Arenholz, V. A. Stoica, S.-L. Hsu, B. Wang, C. Ophus, J. F. Liu, C. T. Nelson, S. Saremi, B. Prasad, A. B. Mei, D. G. Schlom, J. Íñiguez, P. García-Fernández, D. A. Muller, L. Q. Chen, J. Junquera, L. W. Martin, R. Ramesh, Nature 568, 368–372 (2019).

[35] Q. Zhang, L. Xie, G. Liu, S. Prokhorenko, Y. Nahas, X. Pan, L. Bellaiche, A. Gruverman, N. Valanoor, Adv. Mat 29, 1702375, (2017).

[36] S. K. Singh, H. Ishiwara, Appl. Phys. Lett. 88, 262908 (2006).

[37] X. H. Zhu, H. Béa, M. Bibes, S. Fusil, K. Bouzehouane, E. Jacquet, A. Barthélémy, D. Lebeugle, M. Viret, D. Colson, Appl. Phys. Lett. 93, 082902 (2008).

[38] J. Wu, J. Wang, D. Xiao, J. Zhu, ACS Appl. Mater. Interfaces 3, 2504–2511, [2011).

[39] B. Negulescu, J. Wolfman, C. Daumont, N. Jaber, P. Andreazza, T. Denneulin, S. Schamm-Chardon, Appl. Surf. Sci. 481, 234–240, (2019).

[40] C. Daumont, J. Wolfman, C. Autret-Lambert, P. Andreazza, B. Negulescu, Appl. Phys. Lett. 112, 112401, (2018).

[41] N. Bassiri-Gharb, I. Fujii, E. Hong, S. Trolier-McKinstry, D. V. Taylor, D. Damjanovic, J Electroceram. 19, 47-65, (2007).

[42] T. Nan, Z.Y. Zhou, J. Lou, M. Liu, X. Yang, Y. Gao, S. Rand, N.X. Sun, Appl. Phys. Lett., 100, 132409, (2012).

[43] J. M. Hu, L. Shu, Z. Li, Y. Gao, Y. Shen, Y. H. Lin, L. Q.Chen, C. W. Nan, Phil. Trans. R. Soc. A 372, 20120444, (2014).

[44] M. Huijben, P. Yu, L. W. Martin, H. J. A. Molegraaf, Y.-H. Chu, M. B. Holcomb, N. Balke, G. Rijnders, R. Ramesh, Adv. Mat., 25, 4739-4745, (2013).

[45] C. Lichtensteiger, S. Fernandez-Pena, C. Weymann, P. Zubko, J.-M. Triscone, Nano Lett., 14, 4205 −4211, (2014).

[46] C. Lichtensteiger, C. Weymann, S. Fernandez-Pena, P. Paruch. J.-M. Triscone, New J. Phys. 18, 043030, (2016).

[47] G. Liu, J. Chen, C. Lichtensteiger, J.-M. Triscone, P. Aguado-Puente, J. Junquera, N. Valanoor, Adv. Electron. Mater. 2, 1500288, (2016).

[48] D. Chen, Z. Chen, Q. He, J. D. Clarkson, C. R. Serrao, A. K. Yadav, M. E. Nowakowski, Z. Fan, L. You, X. Gao, D. Zeng, L. Chen, A. Y. Borisevich, S. Salahuddin, J.-M. Liu, J. Bokor, Nano Lett., 17, 486−493, (2017).

[49] C. Beekman, W. Siemons, M. Chi, N. Balke, J. Y. Howe, T. Z. Ward, P. Maksymovych, J. D. Budai, J. Z. Tischler, R. Xu, W. Liu, H. M. Christen, Adv. Funct. Mater. 26, 5166–5173, (2016).

[50] S. Y. Lim, M. S. Park, S. Wi, J.-S. Chung, S. M. Yang, Current Appl. Phys., 20, 1185–1189, (2020).

Figures caption

Figure 1: a) Schematic representation of the ME device. b) Ni(30 nm)/ BFMO(60 nm) magnetic hysteresis loops measured in the as deposited state (blue triangles), in the positively poled state obtained by applying +6 V (black circles) and in the negatively poled state induced by -6 V (red squares). Polar plots of Hc (c) and Mr/Ms (d) presented for the three different electric states described in (b).

Figure 2: Variation of the Hc difference between the positively and the negatively poled states in Ni(30 nm)/ STO/ BFMO(60 nm) heterostructures as a function of the STO spacer thickness. Lines are linear fits. The ΔHc value measured in Ni(30 nm)/ BFMO(60 nm) bilayer is also presented (star symbol).

Figure 3: a) Hc (black circles), b) Ms normalized to the Ms value at +6 V (blue rectangles) and c) d_{33} (green triangles) variations with the DC voltage for three different STO spacer thicknesses: 0 nm, 2 nm, and 5.5 nm.

Figure 4: Atomic Force Microscopy image showing the topography (a) and PFM images showing the out-of-plane amplitude contrast (b) and the out-of-plane phase contrast (c) in BFMO film with a STO top layer.

Figure 1

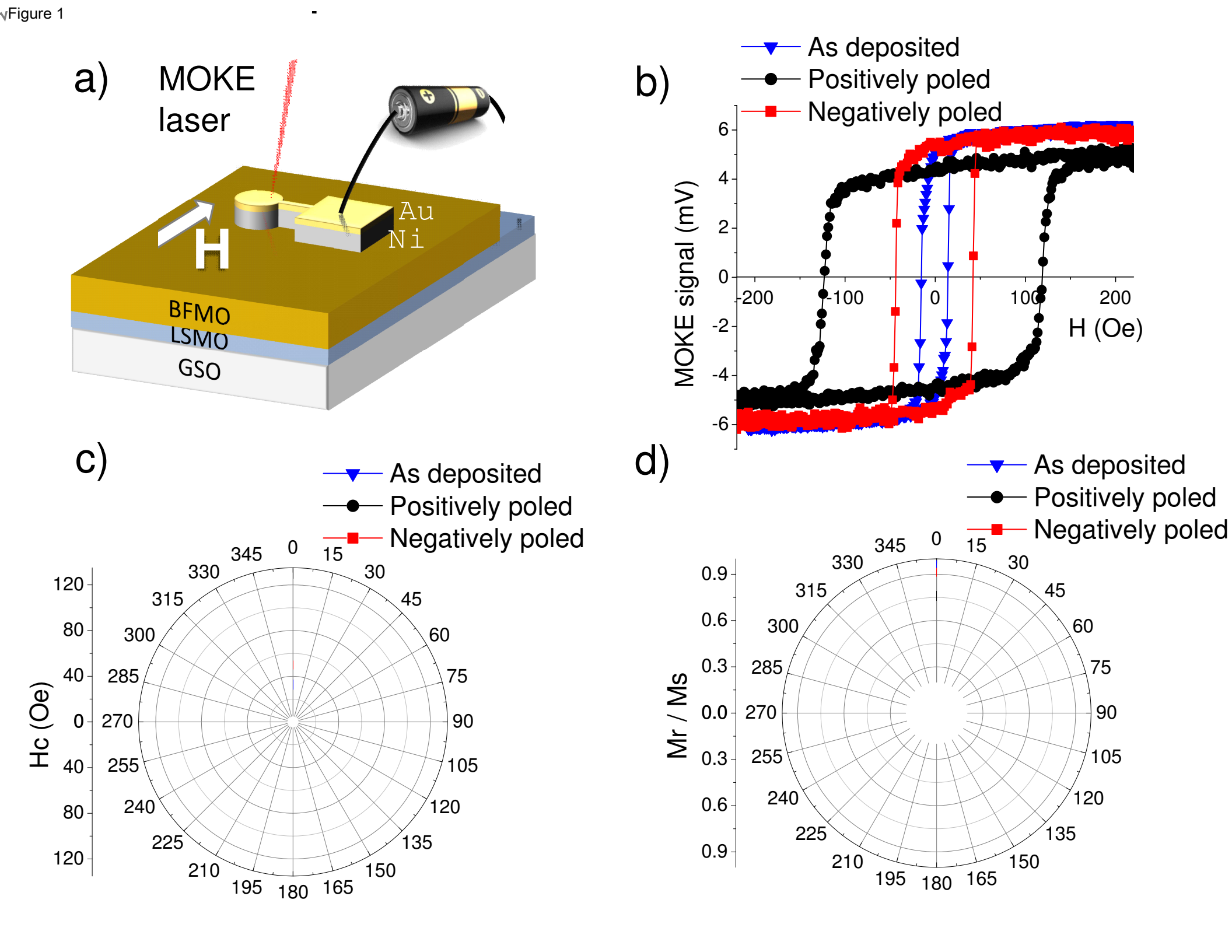
a)
MOKE
laser
H
Au
Ni
BFMO
LSMO
GSO
b)
As deposited
Positively poled
Negatively poled
MOKE signal (mV)
H (Oe)
c)
As deposited
Positively poled
Negatively poled
Hc (Oe)
d)
As deposited
Positively poled
Negatively poled
Mr / Ms

Figure 1

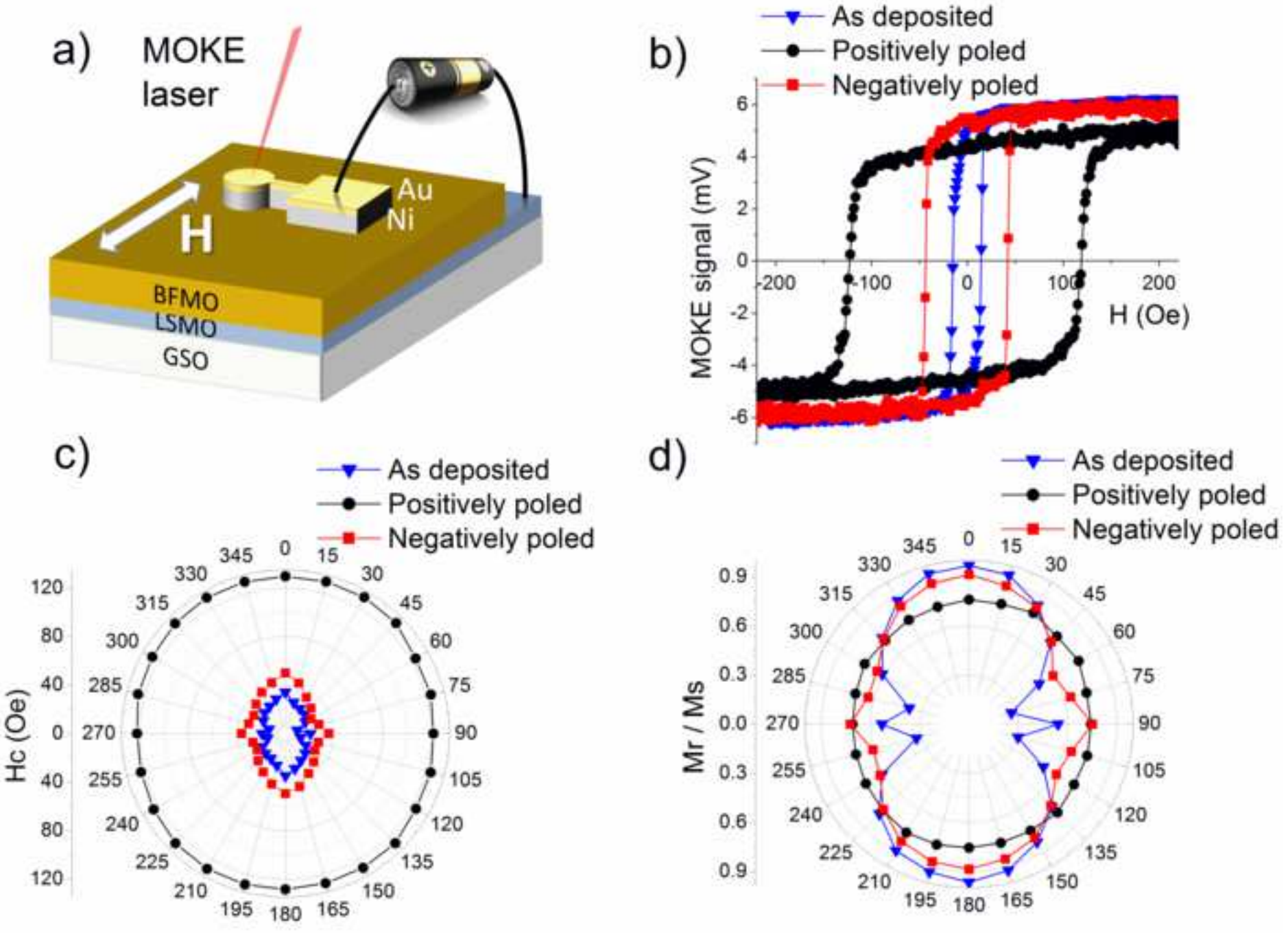
a)
MOKE
laser
Au
Ni
H
BFMO
LSMO
GSO
b)
As deposited
Positively poled
Negatively poled
MOKE signal (mV)
H (Oe)
c)
As deposited
Positively poled
Negatively poled
Hc (Oe)
d)
As deposited
Positively poled
Negatively poled
Mr / Ms

Figure 2

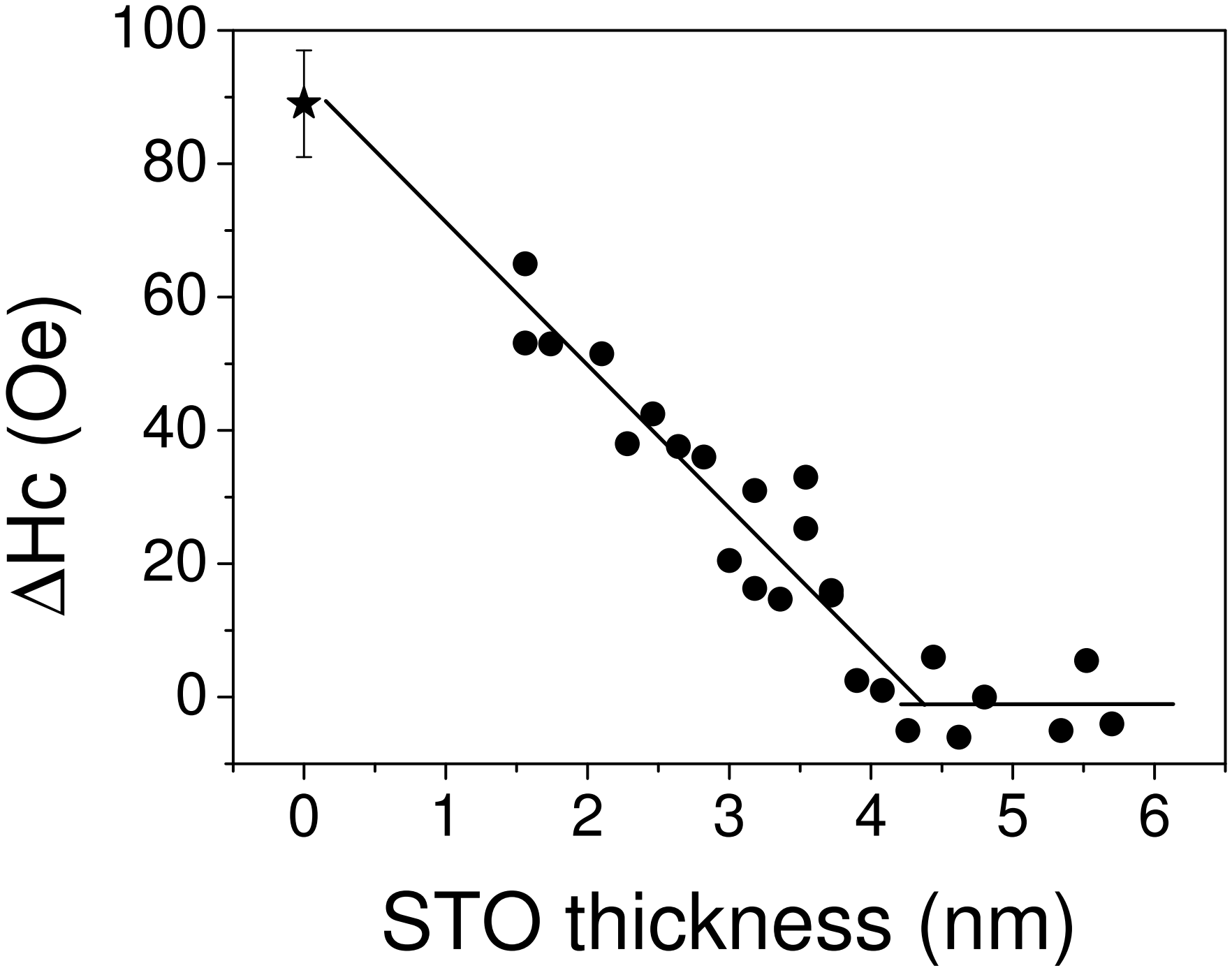

Figure 3

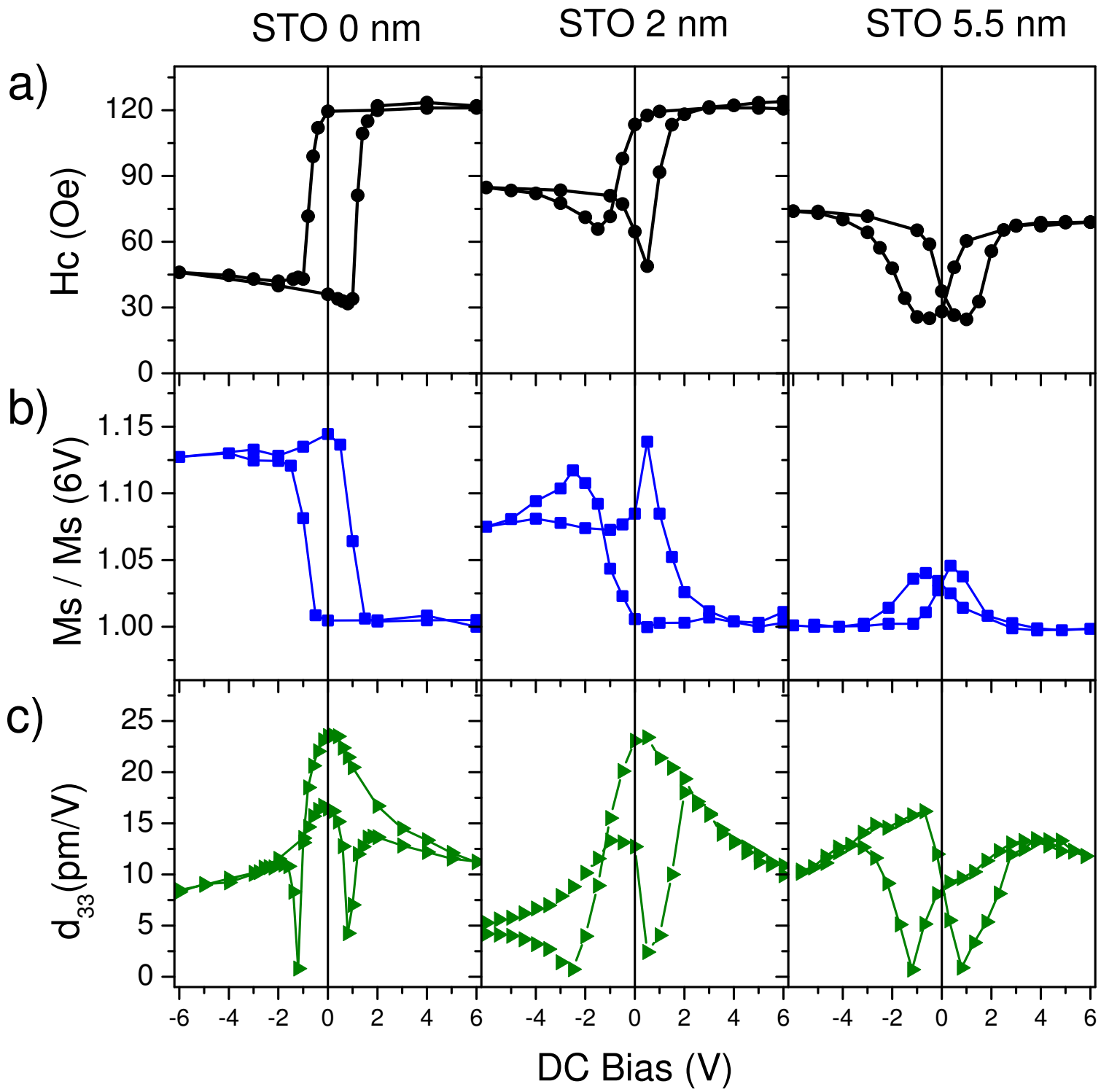
STO 0 nm
STO 2 nm
STO 5.5 nm
a)
Hc (Oe)
120
90
60
30
0
b)
Ms / Ms (6V)
1.15
1.10
1.05
1.00
c)
d33(pm/V)
25
20
15
10
5
0
-6
-4
-2
0
2
4
6
DC Bias (V)

Figure 4

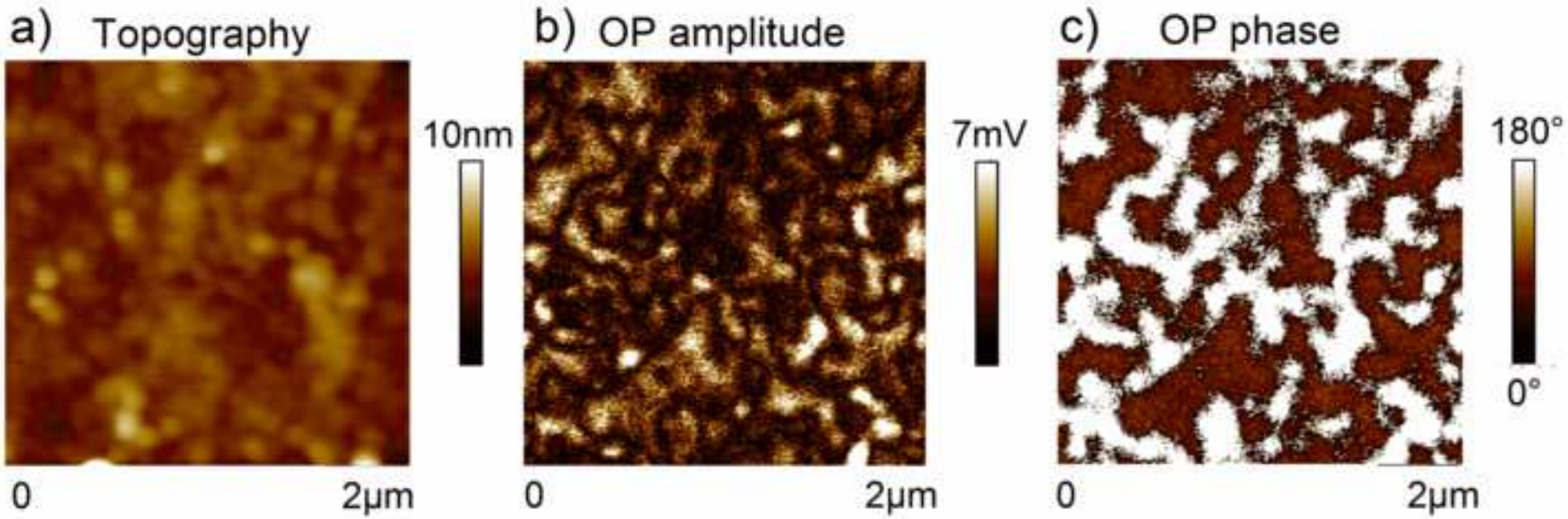
a) Topography
10nm
0
2μm
b) OP amplitude
7mV
0
2μm
c) OP phase
180°
0°
0
2μm

Figure 4

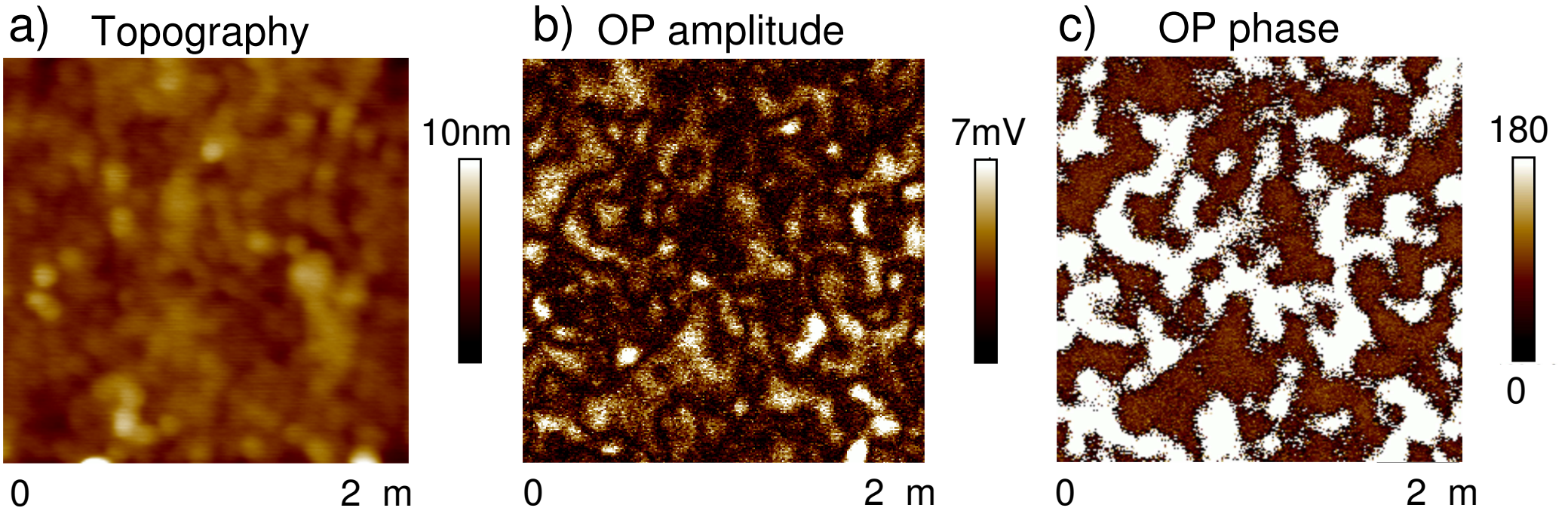
a) Topography
10nm
0
2 m
b) OP amplitude
7mV
0
2 m
c) OP phase
180
0
0
2 m

Declaration of interests

☒ The authors declare that they have no known competing financial interests or personal relationships that could have appeared to influence the work reported in this paper.

☐The authors declare the following financial interests/personal relationships which may be considered as potential competing interests:

Author Statement

Beatrice Negulescu: Conceptualization, Investigation, Formal analysis, Writing - Original Draft, Writing - Review & Editing.
Jérôme Wolfman: Conceptualization, Investigation, Formal analysis, Writing - Original Draft.
Antoine Ruyter: Conceptualization, Formal analysis, Writing - Original Draft.
Cécile Autret - Lambert: Investigation, Formal analysis.
Salia Cherifi - Hertel: Conceptualization, Investigation, Formal analysis, Writing - Original Draft